Chinese Chemical Letters 36 (2025) 110376

Contents lists available at ScienceDirect

Chinese Chemical Letters

journal homepage: www.elsevier.com/locate/cclet

HClO-responsive dinuclear Ru(II) complexes for selective imaging and efficient photo-inactivation of intracellular bacteria

Wanpeng Zhou[a,b], Xuwen Da[a], Yunli Xu[a,b], Yatong Peng[a,b], Xiulian Liu[a,b], Yao Wu[a,b], Yu Shi[a,b], Aifeng Wu[a,b], Yishan Yao[c,*], Xuesong Wang[a,b,*], Qianxiong Zhou[a,*]

[a] Key Laboratory of Photochemical Conversion and Optoelectronic Materials, Technical Institute of Physics and Chemistry, Chinese Academy of Sciences, Beijing 100190, China
[b] University of Chinese Academy of Sciences, Beijing 100049, China
[c] Beijing Institute of Pharmacology and Toxicology, Beijing 100850, China

ARTICLE INFO

Article history:
Received 15 June 2024
Revised 22 August 2024
Accepted 26 August 2024
Available online 28 August 2024

Keywords:
Intracellular bacteria
HClO-responsive
Ru(II) complexes
Antibacterial photodynamic therapy
Selective imaging and photo-inactivation

ABSTRACT

Intracellular bacteria (ICB), cloaked by the protective barriers of host cells, pose a formidable challenge to selective and efficient eradication. The employment of activatable photosensitizers based antibacterial photodynamic therapy (aPDT) holds significant potential for selective imaging and photo-inactivation of ICB while minimizing side effects on normal cells. Drawing inspiration from the elevated hypochlorous acid (HClO) levels in ICB infected phagocytes, herein we firstly designed and synthesized a series of HClO-responsive dinuclear Ru(II) complexes (Ru1-Ru3) to achieve such a goal. Initially, the luminescence, $^1O_2$ generation and aPDT activity of these Ru(II) complexes were suppressed due to the quenching effect of the azo group, but were recovered after reaction with HClO in solutions or within ICB infected phagocytes. The detailed results revealed that Ru1 and Ru3 could not only selectively visualize ICB, but also demonstrated remarkable aPDT activity against ICB, surpassing vancomycin both *in vitro* and *in vivo*.

Staphylococcus aureus (*S. aureus*) affects approximately one-third of the world's population and can cause severe and life-threatening infections such as abscesses, endocarditis, pneumonia, toxic shock syndrome and sepsis [1]. The situation is getting worse due to the escalating prevalence of antibiotic resistance. For example, methicillin-resistant *S. aureus* (MRSA), has developed resistance to almost all clinically approved antibiotics so far [2-4]. Moreover, *S. aureus* is capable of invading and surviving inside host cells (including phagocytes cells) to form intracellular bacteria (ICB) [5], which protects them from damages by antibiotics and immune system [6-8]. Despite the availability of numerous effective antibiotics against extracellular bacteria, the options for treating ICB infections remain highly limited due to the poor membrane permeability [9,10]. To address this issue, various drug delivery systems are explored for ICB treatment, such as antibody–antibiotic conjugates [11], cell-mediated drug delivery carriers [12,13], and drug-loaded nanosystems [14,15]. While the aforementioned platforms exhibit promising potential, they still face several limitations, including complex synthesis procedures, the absence of diagnostic functionality, and ineffectiveness against drug-resistant ICB strains.

Antibacterial photodynamic therapy (aPDT) has attracted much attention in recent years [16-20]. The three main components of aPDT are light, photosensitizer (PS), and oxygen, which work together to produce highly toxic reactive oxygen species (ROS). ROS can cause damage to multiple bacterial targets, such as cell membrane, proteins, and DNA, among others [21], thus posing a significant challenge for bacteria to develop resistance to aPDT. However, the "always on" characteristics of common PSs and highly toxic ROS can also cause damages towards normal tissues by either treatment light or daylight. Therefore, design of stimuli-responsive aPDT agents is more promising for selective imaging and photo-inactivation of ICB. Recently, some aPDT agents have been reported to fulfill this function [22-26]. For example, Liu *et al.* reported a D-alanine modified aggregation induced emission (AIE) probe (TPEPy-D-Ala), which could metabolically incorporate into bacterial peptidoglycan and realize fluorescence turn-on imaging and photodynamic ablation of ICB [23]. They also synthesized AIE PSs that can respond to caspase-1 overexpressed in infected phagocytes, realizing selective imaging and photodynamic ablation of ICB [24]. According to the overexpression of nitroreductase (NTR) in *S. aureus*, our group has developed NTR responsive PSs for selective imaging

* Corresponding authors.
E-mail addresses: spray_yao123456@hotmail.com (Y. Yao), xswang@mail.ipc.ac.cn (X. Wang), zhouqianxiong@mail.ipc.ac.cn (Q. Zhou).

https://doi.org/10.1016/j.cclet.2024.110376
1001-8417/

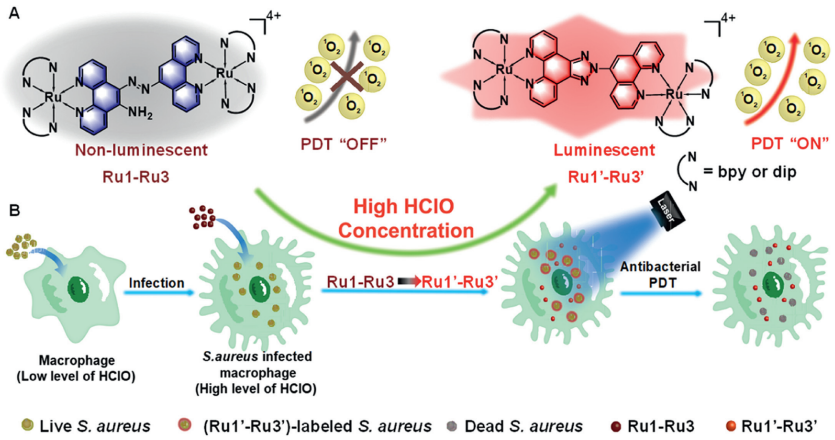

Scheme 1. Schematic illustration of HClO responsive PSs for selective imaging and photo-inactivation of ICB. (A) The response mechanism of Ru1-Ru3 towards HClO. (B) Photo-inactivation of intracellular *S. aureus* by Ru1-Ru3 *in vitro*.

and photo-inactivation of intracellular *S. aureus* [25]. Wang *et al.* designed macrophage-instructed peptide–chlorophyll-based dimers with active targeting property that can produce singlet oxygen to kill intracellular *S. aureus* under irradiation [26]. These works have demonstrated the superiority of stimuli-responsive aPDT agents for selective photo-inactivation of ICB, yet such advancements remain relatively rare.

A large number of studies have shown that endogenous hypochlorous acid (HClO) level within phagocytes (including macrophages and neutrophils) is significantly elevated due to bacterial invasion [27,28]. Endogenous HClO is produced by the oxidation of chloride ions catalyzed by myeloperoxidase [29,30], and holds a pivotal position in the immune system, particularly against invading bacteria [31]. However, the specific secretion systems of ICB enable them to evade the lethal effects of HClO and survive within host phagocytic cells [32]. Even so, the elevated HClO level can still be served as a specific biomarker for diagnosing ICB infections. In recent years, a diverse array of probes has been developed for imaging intracellular HClO [33-37]. However, there has been only one instance where such a probe could be utilized concurrently for selective photo-inactivation of ICB [35].

In recent years, Ru(II) polypyridyl complexes have attracted significant attention for biological applications, primarily due to their exceptional photophysical and chemical properties [18,20,38,39]. In this work, we have designed and synthesized, for the first time, a series of HClO-responsive dinuclear Ru(II) complexes (Ru1-Ru3, Scheme 1 and Scheme S1 in Supporting information) for selective imaging and photo-inactivation of ICB. The *o*-amino azo group on the bridge ligand serves as a recognition site for HClO and also a quenching group of ^{3}MLCT (metal-to-ligand charge transfer) state [37], leading to weak luminescence and low $^1O_2$ generation efficiency of Ru1-Ru3. However, upon reacting with HClO, the *o*-amino azo group is oxidatively cyclized and converted to benzotriazole, and the resultant compounds (Ru1'-Ru3') demonstrate pronounced luminescence and high $^1O_2$ quantum yields. Ru1 and Ru3 display quite low dark- and photo-cytotoxicity towards normal mammalian cells, but can selectively visualize and efficiently photo-inactivate ICB both *in vitro* and *in vivo*.

As demonstrated in Scheme S1, the bridging ligand phen-azo was facilely synthesized by a one-step reaction procedure. Then, by maintaining the bridging ligand as the recognition site for HClO while varying the auxiliary ligands attached to the Ru(II) center, it is facile to adjust the lipophilicity of Ru(II) complexes without altering their HClO responsiveness. Specifically, the hydrophilic 2,2′-bipyridine (bpy) and hydrophobic 4,7-diphenyl-1,10-phenanthroline (dip) were selected as auxiliary ligands, and three new complexes Ru1-Ru3 were prepared. All compounds were characterized by ^{1}H nuclear magnetic resonance spectroscopy (NMR), ^{13}C NMR, high-resolution electrospray ionization mass spectrometry (HR ESI-MS) and high performance liquid chromatography (HPLC) (Figs. S1–S15 in Supporting information). Among them, Ru3 is potentially a mixture of two isomers, but cannot be purified by general column chromatography probably due to the extremely similar polarity.

Ru1 coordinated with bpy exhibits excellent hydrophilicity (Log*P* = −2.52), while Ru2 coordinated with dip demonstrates strong lipophilicity (Log*P* = 1.13). Ru3, which is coordinated with both dip and bpy, falls somewhere between these two extremes (Log*P* = −0.58). The variations in their lipophilicity may have a notable impact on their cellular uptake, distribution, metabolism, and toxicity [40].

HClO response of Ru1-Ru3 was firstly investigated by emission and absorption spectra. As shown in Figs. 1A–C, Ru1-Ru3 exhibited quite weak luminescence in water. However, upon gradual addition of HClO (ranging from 0 to 100 μmol/L), the luminescence intensity was significantly enhanced for about 110, 20 and 21 times for Ru1-Ru3, respectively. Meanwhile, the absorbance of Ru1-Ru3 among 400–550 nm gradually decreased (Fig. S16 in Supporting information). In addition, the luminescence intensity of Ru1-Ru3 at 625 nm showed a good linear relationship with the concentration of HClO (Fig. S17 in Supporting information). Based on these data, the limit of detection (LOD, $3\sigma/k$) and limit of quantification (LOQ, $10\sigma/k$) values of Ru1, Ru2 and Ru3 were calculated to be 0.028 and 0.093 μmol/L, 1.26 and 4.21 μmol/L, 0.20 and 0.67 μmol/L, respectively [41,42]. To further explore the specificity, the luminescence intensity of Ru1-Ru3 at 625 nm towards various substances, including ROS (such as $^1O_2$, $^{\bullet}OH$), reductive species (such as vitamin C, L-glutathione (GSH)), amino acids (such as L-Arg, L-Glu), metal ions (such as Fe^{2+}, Fe^{3+} and K^+), and some anions (such as SO_4^{2-}, $S_2O_3^{2-}$ and SCN^-) was also investigated. As shown in Fig. 1D and Fig. S18 (Supporting information), a significant enhancement in luminescence is observed solely upon addition of HClO, indicating the good selectivity of Ru1-Ru3 towards HClO.

To facilitate experimentation in subsequent studies, the crude compounds Ru1'-Ru3' were prepared by stirring Ru1-Ru3 with NaClO (10 equiv.) in a CH_3CN/H_2O (1/1) solution. Excess NaClO was then removed through water washing. After that, the ESI-MS spectra clearly displayed Ru1'-Ru3' based signals (Figs. S19–S21 in Supporting information), and the ^{1}H NMR spectra indicated the full conversion of Ru1-Ru3 in the presence of NaClO (Figs. S22–S24 in Supporting information). Then, the emission quantum yields of Ru1-Ru3 and Ru1'-Ru3' were determined using $[Ru(bpy)_3]Cl_2$ as a reference ($\varphi = 0.042$ in H_2O) [43]. Ru1-Ru3 are almost non-

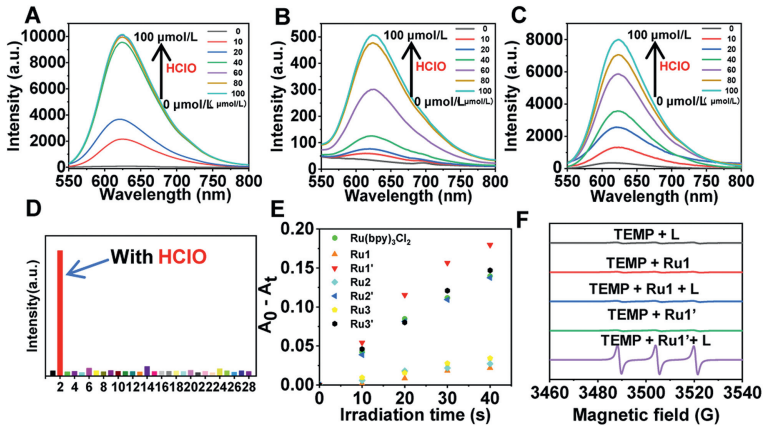

Fig. 1. Emission spectra of Ru1 (A), Ru2 (B) and Ru3 (C) (10 μmol/L) upon treatment with HClO (0–100 μmol/L). (D) Emission intensity at 625 nm of Ru1 (10 μmol/L) incubated with various species (100 μmol/L) including blank (1), HClO (2), H_2O_2 (3), *t*Bu-OOH (4), $O_2^{-\bullet}$ (5), ·OH (6), $ONOO^-$ (7), $^1O_2$ (8), vitamin C (9), GSH (10), cysteine (11), L-Arg (12), L-Glu (13), Fe^{2+} (14), Fe^{3+} (15), K^+ (16), Na^+ (17), Mg^{2+} (18), Zn^{2+} (19), Ca^{2+} (20), Cu^{2+} (21), Cu^+ (22), SO_4^{2-} (23), $S_2O_3^{2-}$ (24), SCN^- (25), NO_2^- (26), HSO_3^- (27), and Cl^- (28). (E) Irradiation (470 nm, 22.5 mW/cm^2) induced absorbance (378 nm) changes of 9,10-ADPA in the presence of Ru1-Ru3 and Ru1'-Ru3'. (F) EPR spectra of Ru1 and Ru1' in water with or without light irradiation (470 nm LED, 22.5 mW/cm^2) using TEMP as the singlet oxygen trap. "L" denotes "light irradiation".

emissive in water, with quantum yields of about 5.03×10^{-4}, 2.55×10^{-4} and 2.17×10^{-3}, respectively. In contrast, Ru1'-Ru3' displayed much higher luminescent intensity with quantum yields of 0.063, 0.0046 and 0.061, respectively.

In addition, the $^1O_2$ generation capacity of Ru1-Ru3 and Ru1'-Ru3' were determined using 3,3′-(anthracene-9,10-diyl)dipropanoic acid (9,10-ADPA) as a probe. The absorbance at 378 nm of 9,10-ADPA will decrease after reacting with $^1O_2$ [44]. As shown in Fig. 1E, Ru1-Ru3 exhibited poor $^1O_2$ generation ability, with quantum yields of about 7%, 8% and 9%, respectively, using $[Ru(bpy)_3]Cl_2$ as a reference (41% in H_2O) [45]. In contrast, Ru1'-Ru3' displayed much more effective $^1O_2$ production as they could quickly bleach the absorbance of 9,10-ADPA upon irradiation. The $^1O_2$ quantum yields of Ru1'-Ru3' were estimated to be about 54%, 41% and 43%, respectively. Furthermore, $^1O_2$ generation was characterized by electron paramagnetic resonance (EPR) spectra, employing 2,2,6,6-tetramethyl-4-piperi-dinol (TEMP) as a spin trapping agent. As shown in Fig. 1F and Fig. S25 (Supporting information), neither irradiation alone nor the presence of the complexes without irradiation led to a significant enhancement in the TEMPO (product of the reaction between TEMP and $^1O_2$) signal. A slight enhancement in the TEMPO signal was observed when Ru1-Ru3 were irradiated, indicating their relatively limited $^1O_2$ generation capacity. However, a substantial increase in the TEMPO signal was evident for Ru1'-Ru3', which aligns with their much higher $^1O_2$ quantum yields.

In order to better understand the photophysical properties of Ru1-Ru3 before and after reaction with HClO, theoretical calculations were carried out taking Ru1 and Ru1' as representatives. The ground-state molecular geometries of Ru1 and Ru1' (Fig. S26 in Supporting information) were optimized based on density functional theory (DFT) calculations, and their representative frontier molecular orbital distributions are shown in Figs. S27 and S28 (Supporting information). Time-dependent density functional theory (TD-DFT) calculations were further employed to investigate the excited properties. The low-lying singlet excited states of Ru1 are mainly ML"CT (L": azo group of the bridging ligand) based (Table S1 and Fig. S29 in Supporting information), and those for Ru1' can be primarily classified as MLCT/ML'CT (L: Phen of the bridging ligand; L': bpy) (Fig. S30 in Supporting information). The triplet states of Ru1 and Ru1' were also calculated (Table S2 and Figs. S31, S32 in Supporting information). The first and second lowest lying triplet excited states (T_1 and T_2) of Ru1 can be attributed to L"-centered (L"C) transitions (Fig. 2A), which sets it apart from typical

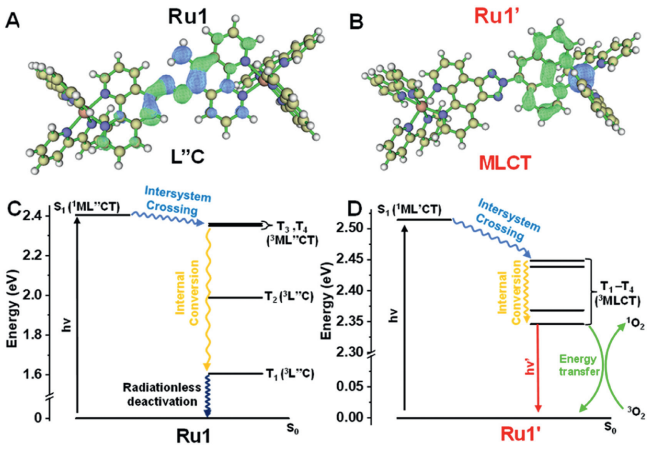

Fig. 2. Real space representation of hole and electron distributions of Ru1 (A) and Ru1' (B) at T_1 state (isovalue = 0.002, green and blue regions denote the electron and hole distributions, respectively). The simplified diagram of excited state deactivation of Ru1 (C) and Ru1' (D).

Ru(II) polypyridine complexes where ^{3}MLCT typically serves as the lowest excited state. Additionally, the third and fourth lowest-lying states (T_3 and T_4) are ^{3}ML"CT based,exhibiting an energy gap of over 0.7 eV compared to T_1. Therefore, thermodynamically allowed energy transfer from ^{3}ML"CT to L"C can be expected, resulting in the radiationless deactivation of the ^{3}ML"CT excited states of Ru1 (Fig. 2C). In contrast, the ^{3}MLCT of Ru1' occupies the lowest triplet excited state (Fig. 2B), which enable it to not only produce $^1O_2$ through energy transfer but also emit luminescence (Fig. 2D).

Since it has been confirmed that the $^1O_2$ generation ability of Ru1-Ru3 is significantly improved after reacting with HClO, thus the different aPDT activity of Ru1-Ru3 and Ru1'-Ru3' against extracellular *S. aureus* and MRSA was investigated. As expected, Ru1-Ru3 exhibited low aPDT activity due to the poor $^1O_2$ generation ability, whereas Ru1'-Ru3' showed high antibacterial efficacy under irradiation conditions (470 nm, 22.5 mW/cm^2) (Figs. S33 and S34 in Supporting information). 10 μmol/L of Ru1'-Ru3' could lead to a colony-forming unit (CFU) reduction of about 3–4 log units against *S. aureus* and MRSA.

For aPDT agents, good biocompatibility is a prerequisite for clinical application. Selective sterilization without causing damage to normal cells is important. As a representative of mammalian cells,

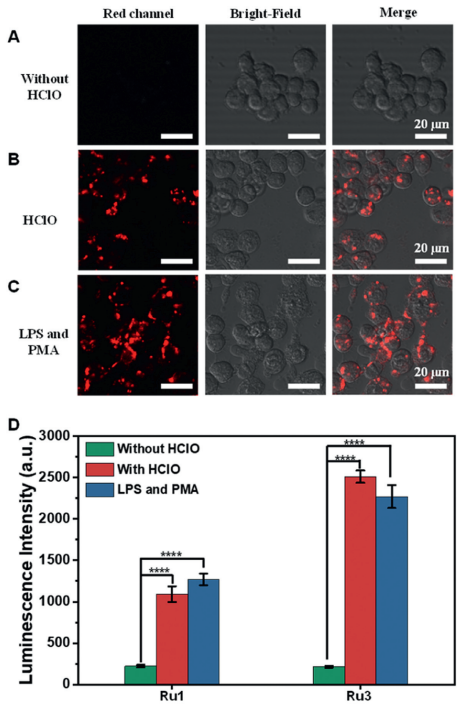

Fig. 3. (A) CLSM images of RAW 264.7 cells incubated with Ru1. (B) CLSM images of RAW 264.7 cells treated with Ru1 and subsequent addition of HClO. (C) CLSM images of RAW 264.7 cells firstly treated with LPS and PMA, and subsequently treated with Ru1. (D) Quantized red luminescence intensity of RAW 264.7 cells after different treatments. [Ru1] = 10 μmol/L, [HClO] = 100 μmol/L, [LPS] = 1 μg/mL, [PMA] = 10 μg/mL. The red channel was excited at 488 nm and collected at 570–620 nm. Data are presented as mean ± standard deviation (SD) ($n = 3$). $^{****}P < 0.0001$.

human normal liver cells (L-O2) were selected for cytotoxicity test through MTT assay. As shown in Fig. S35 (Supporting information), Ru1 and Ru3 exhibited negligible cytotoxicity with or without irradiation, maintaining cell survival rates above 90% even at a concentration of 20 μmol/L. Conversely, Ru2 displayed significant cell toxicity under identical conditions, potentially due to its excessive lipophilicity and consequent much enhanced cell uptake. To further assess the biocompatibility of Ru1 and Ru3, we measured their hemolysis rates. As shown in Fig. S36 (Supporting information), the hemolysis rates of Ru1 and Ru3 towards rabbit red blood cells (RBCs) were only 1.9% and 2.4% even at 20 μmol/L. Given the good biocompatibility of Ru1 and Ru3, they were selected for the following investigations.

The HClO response of Ru1 and Ru3 within monocyte macrophage (RAW 264.7) cells was studied by confocal laser scanning microscope (CLSM). As shown in Fig. 3A and Fig. S37A (Supporting information), after incubation with 10 μmol/L of Ru1 or Ru3 for 2 h, no significant luminescence was observed within RAW 264.7 cells. However, upon addition of HClO, intense red emission was observed in both Ru1 and Ru3 cultured cells, indicating their excellent response to intracellular HClO (Fig. 3B and Fig. S37B in Supporting information). Furthermore, the response towards endogenous HClO within cells was also examined. It has been reported that lipopolysaccharide (LPS) and phorbol myristate acetate (PMA) could effectively stimulate macrophages to generate endogenous HClO [46]. Thus RAW 264.7 cells were consecutively treated with LPS and PMA, subsequently were incubated with Ru1 and Ru3 for 2 h. Notably, a substantial enhancement in red luminescence was observed (Fig. 3C and Fig. S37C in Supporting information). Under the same treatment conditions, the luminescence intensity of Ru3 is approximately twice that of Ru1 (Fig. 3D). Given the similar emission quantum yields of Ru1' and Ru3' ($\varphi = 0.063$ and 0.061), we tentatively attribute this difference to the higher lipophilicity of Ru3, which leads to increased cellular uptake compared to Ru1.

As a pivotal biomarker of ICB infection, the concentration of HClO in phagocytic cells is known to increase significantly following bacterial invasion, suggesting the possibility that Ru1 and Ru3 have potential for imaging ICB infections. To explore the feasibility, RAW 264.7 cells were infected with fluorescein isothiocyanate (FITC)-labeled *S. aureus* to stimulate HClO generation. Subsequently, the cells were treated with Ru1 or Ru3 (10 μmol/L) for 2 h and then were investigated by CLSM. As shown in Fig. 4A, green fluorescence of FITC is clearly visible in RAW 264.7 cells, indicating successful formation of intracellular *S. aureus* infections. In this case, obvious red luminescence of Ru1' and Ru3' formed *in situ* was also observed. This suggests significant endogenous HClO is produced due to ICB infections, which converts the almost non-luminescent Ru1 and Ru3 into emissive Ru1' and Ru3'. Additionally, the line-scan profiles show that the red luminescence fits well with the green fluorescence of *S. aureus* (Figs. 4B and C). Moreover, the intensity scatter plots of the red channel and green channel are well correlated with high overlap Pearson's coefficients of 0.947 and 0.957 (Figs. 4D and E). These results indicate that Ru1 and Ru3 can well bind with intracellular *S. aureus*. Bacteria are generally negatively charged [47,48], thus Ru1 and Ru3 with four positive charges may bind with *S. aureus* through electrostatic interaction. To confirm our inference, the impact of Ru1 and Ru3 on the zeta potential of *S. aureus* was investigated, and $[Ru(bpy)_3]Cl_2$, the representative of mononuclear Ru(II) polypyridyl complex with only two positive charges, was also studied as a control. The measured average zeta potential value of *S. aureus* is about -40.2 ± 0.4 mV, in accordance with its negatively charged cell wall. Incubation with Ru1 or Ru3 (10 μmol/L) resulted in a significant positive shift to -38.1 ± 0.5 and -37.4 ± 0.8 mV, respectively. In contrast, only a slight shift to -39.8 ± 0.7 mV was obtained for *S. aureus* treated with $[Ru(bpy)_3]Cl_2$. Given that $[Ru(bpy)_3]Cl_2$ demonstrates comparable hydrophilicity ($LogP = -2.72$) to Ru1, the increased positive charge of Ru1 and Ru3 should play an important role for the remarkable bacterial binding capacity.

The remarkable response of Ru1 and Ru3 towards intracellular HClO and efficient aPDT activity of Ru1'-Ru3' against extracellular bacteria stimulate us to investigate their performance to eliminate intracellular *S. aureus*. Firstly, to investigate the intracellular ROS generation for RAW 264.7 cells successively treated with *S. aureus* and Ru1 or Ru3, DCFH-DA was used as a ROS indicator. DCFH-DA is non-emissive but exhibits strong green fluorescence after reaction with ROS [49]. As shown in Fig. 5A, the DNA of intracellular *S. aureus* and RAW 264.7 cells were stained with Hoechst 33342, and the red arrows indicated the presence of intracellular *S. aureus*. After irradiation, intense green fluorescence was mainly observed in proximity to the bacteria, which indicates efficient ROS production within intracellular *S. aureus* and is consistent with the good bacterial targeting ability of Ru1 and Ru3 observed in Fig. 4A. The control experiments display that light irradiation, Ru1/Ru3 and *S. aureus* are all necessary for ROS production (Fig. S38 in Supporting information). The efficient ROS production of Ru1 and Ru3 within ICB-infected cells indicates their potential for photo-elimination of intracellular *S. aureus*. To quantify this effect, the bacterial colony counting method was employed, and the widely used antibiotic vancomycin (Van) was also used as a control. As shown in Fig. 5B, Ru1 and Ru3 upon light irradiation (470 nm, 22.5 mW/cm^2) exhibit significantly better performance than Van, while Ru3 is slightly better than Ru1. Specifically, at a concentration of 10 μmol/L, Ru1 and Ru3 reduced intracellular *S. aureus* by approximately 90% and 95%, respectively. In contrast, Van only achieved an about 80% elimination rate. Interestingly, Ru1 and Ru3 also exhibited similar

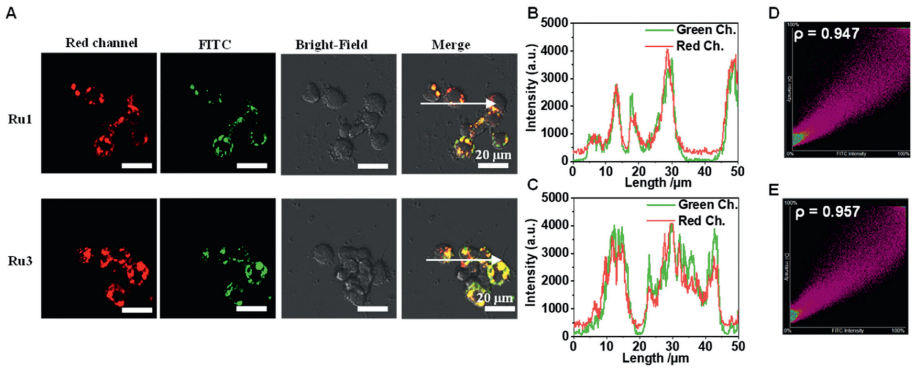

Fig. 4. (A) CLSM images of RAW 264.7 cells which were firstly infected with FITC-labeled *S. aureus*, then were incubated with Ru1 or Ru3 (10 μmol/L). Line-scan profiles of RAW 264.7 cells co-stained with green channels of FITC and red channels of Ru1 (B) or Ru3 (C). Intensity scatter plots of green and red channels of the cells treated with Ru1 (D) or Ru3 (E).

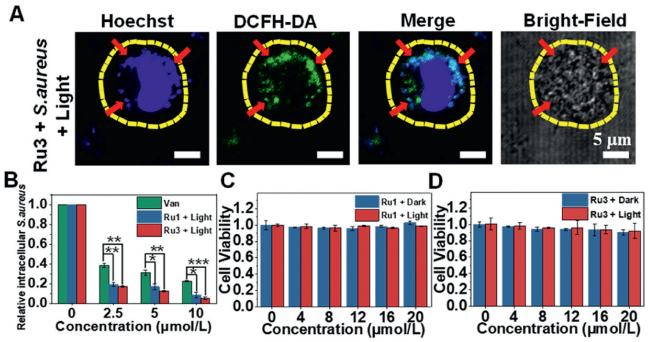

Fig. 5. (A) CLSM images of ROS production within RAW 264.7 cells successively treated with *S. aureus* and Ru3. DCFH-DA was used as the ROS probe and Hoechst was applied to stain the bacterial and host cell DNA. The red arrows indicate the presence of *S. aureus*. (B) Relative recovered intracellular *S.aureus* after different treatments. Cytotoxicity of Ru1 (C) and Ru3 (D) towards RAW 264.7 cells. Irradiation conditions: 470 nm LED, 22.5 mW/cm^2, 20 min. Data arepresented as mean ± SD ($n = 3$). $^*P < 0.05$, $^{**}P < 0.01$, $^{***}P < 0.001$.

activity towards intracellular MRSA (Fig. S39 in Supporting information). Additionally, Ru1 and Ru3 also displayed negligible cytotoxicity towards RAW 264.7 cells with or without irradiation (Figs. 5C and D), consistent with their excellent biocompatibility.

Given the superior aPDT effect of Ru3 against intracellular *S. aureus in vitro*, we proceeded to investigate the performance *in vivo*. All animal experiments were carried out with the permission of the Ethics Committee of Technical Institute of Physics and Chemistry, CAS (LHDW-24003). *S. aureus*-infected RAW 264.7 cells were injected into the upper right leg of female BALB/c nude mice, and simultaneously an equal number of uninfected RAW 264.7 cells were injected into the upper left leg as a control (Fig. 6A). Luminescence imaging was performed 2 h after the *in situ* injection of Ru3. As shown in Figs. 6B and C, no significant luminescence was observed in the left region (control), whereas a pronounced emission was detected in the right region, approximately 3.5 times stronger than that in the left. Furthermore, female BALB/c mice subcutaneously injected with *S. aureus*-infected RAW 264.7 cells were employed as an animal ICB infection model (Fig. 6A). After 12 h, the mice were randomly divided into four groups, with five mice in each group. Then, 50 μL of Ru3 or Van (500 μmol/L), or 50 μL of phosphate buffered saline (PBS), were subcutaneously injected at the infection site. One hour after injection, the light groups were exposed to a 520 nm laser for 10 min (200 mW/cm^2). After 24 h, all mice were sacrificed, and the infected tissues were collected for quantitative assessment of the aPDT effect. As shown in Fig. 6D, Ru3 upon irradiation could kill about 87% of intracellular *S. aureus*, much better than that (about 70%) of Van. As expected,

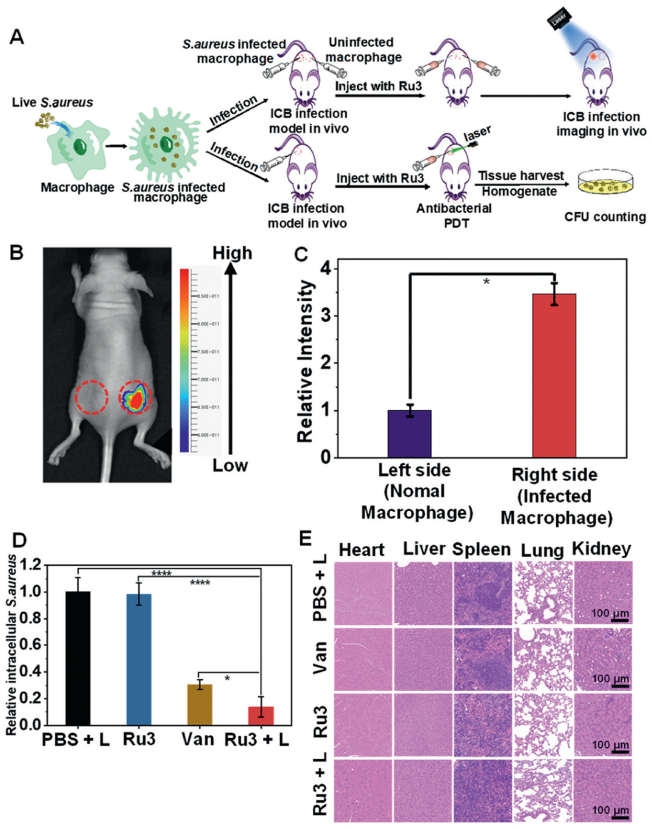

Fig. 6. (A) Schematic illustration of the procedure for imaging and aPDT treatment of ICB infection *in vivo*. A luminescence image (B) and corresponding quantitative analysis of relative luminescence intensity (C) of two regions treated with RAW 264.7 or *S. aureus*-infected RAW 264.7 cells followed by injection of Ru3, the regions injected with RAW 264.7 cells or *S. aureus* infected RAW 264.7 cells were labeled with red circles. (D) *In vivo* antibacterial activities against intracellular *S. aureus* upon different treatments; (E) Representative images of H&E-stained heart, liver, spleen, lung, and kidney of mice after different treatments. Irradiation conditions: 520 nm LED, 200 mW/cm^2, 10 min. Data are presented as mean ± SD ($n = 5$). $^*P < 0.05$, $^{****}P < 0.0001$.

Ru3 without light irradiation did not display significant antibacterial effect. The hematoxylin and eosin (H&E) images of the main organs did not show any abnormalities (Fig. 6E), consistent with the good biocompatibility of Ru3. Overall, these results demonstrate that Ru3 is able to selectively image and efficiently photoinactivate ICB *in vivo*.

In conclusion, a series of HClO-responsive dinuclear Ru(II) complexes (Ru1-Ru3) have been designed and synthesized for selective

imaging and efficient treatment of ICB infection. Ru1-Ru3 display weak luminescence and poor singlet oxygen generation due to the quenching effect of the azo group, therefore exhibit low dark- and photo-cytotoxicity towards mammalian cells especially for Ru1 and Ru3. However, the luminescence, singlet oxygen generation and aPDT activity of Ru1-Ru3 were recovered after reaction with HClO in solutions or within ICB-infected phagocytes. Therefore, Ru1 and Ru3 could selectively visualize and efficiently photo-inactivate intracellular *S. aureus* and MRSA both *in vitro* and *in vivo*, being much more efficient than vancomycin. However, 520 nm light is relatively short for bio-application. Two-photon excitation or combination with upconversion nano-materials are feasible methods to extend the excitation light to near infrared region, which will be investigated in the following work. Nevertheless, to the best of our knowledge, this is the first report of HClO-responsive Ru(II) complexes for innovative theranostic applications related to ICB infections, which may open new ideas for developing novel activatable photosensitizers against intractable ICB.

Declaration of competing interest

The authors declare that they have no known competing financial interests or personal relationships that could have appeared to influence the work reported in this paper.

CRediT authorship contribution statement

Wanpeng Zhou: Writing – original draft, Visualization, Supervision, Investigation, Formal analysis, Data curation, Conceptualization. **Xuwen Da:** Formal analysis. **Yunli Xu:** Formal analysis. **Yatong Peng:** Visualization, Formal analysis. **Xiulian Liu:** Formal analysis, Conceptualization. **Yao Wu:** Software, Formal analysis. **Yu Shi:** Investigation, Conceptualization. **Aifeng Wu:** Methodology, Formal analysis. **Yishan Yao:** Funding acquisition. **Xuesong Wang:** Writing – review & editing, Funding acquisition. **Qianxiong Zhou:** Writing – review & editing, Supervision, Project administration.

Acknowledgment

This work was financially supported by National Natural Science Foundation of China (No. 22371289).

Supplementary materials

Supplementary material associated with this article can be found, in the online version, at doi:10.1016/j.cclet.2024.110376.

References

[1] A.F. Brown, J.M. Leech, T.R. Rogers, R.M. McLoughlin, Front. Immunol. 4 (2014) 507.
[2] G.K. Siberry, T. Tekle, K. Carroll, J. Dick, Clin. Infect. Dis. 37 (2003) 1257–1260.
[3] J.B. Patel, R.J. Gorwitz, J.A. Jernigan, Clin. Infect. Dis. 49 (2009) 935–941.
[4] S. Tsiodras, H.S. Gold, G. Sakoulas, et al., Lancet 358 (2001) 207–208.
[5] X. Liu, Q. Deng, L. Zhang, et al., Chem. Commun. 57 (2021) 2903–2906.
[6] S. Barbarot, S. Auziere, A. Gadkari, et al., Allergy 73 (2018) 1284–1293.
[7] M. Moriwaki, K. Iwamoto, Y. Niitsu, et al., Allergy 74 (2018) 560–571.
[8] Z. Tang, S. Liu, N. Chen, et al., Colloids Surf. B: Biointerfaces 205 (2021) 111899.
[9] M. Maurin, D. Raoult, Drugs 52 (1996) 45–59.
[10] P.M. Tulkens, Eur J Clin Microbiol. Infect. Dis. 10 (1991) 100–106.
[11] S.M. Lehar, T. Pillow, M. Xu, et al., Nature 527 (2015) 323–328.
[12] M.H. Xiong, Y.J. Li, Y. Bao, et al., Adv. Mater. 24 (2012) 6175–6180.
[13] E.V. Batrakova, H.E. Gendelman, A.V. Kabanov, Exp. Opin. Drug Deliv. 8 (2011) 415–433.
[14] H. Qi, P. Shan, Y. Wang, et al., Front. Chem. 9 (2021) 775682.
[15] S.M. Hosseini, M. Taheri, F. Nouri, et al., Biomed. Pharmacother. 146 (2022) 112609.
[16] Y. Wu, J. Li, Z. Shen, et al., Angew. Chem. Int. Ed. 61 (2022) e202212386.
[17] M. Piksa, C. Lian, I.C. Samuel, et al., Chem. Soc. Rev. 52 (2023) 1697–1722.
[18] Y. Jian, Z. Jin, S. Qi, et al., Chem. Eur. J. 28 (2021) e202103359.
[19] H. Yuan, B. Wang, F. Lv, et al., Adv. Mater. 26 (2014) 6978–6982.
[20] Y. Feng, W.Z. Sun, X.S. Wang, Q.X. Zhou, Chem. Eur. J. 25 (2019) 13879–13884.
[21] T. Maisch, R.M. Szeimies, G. Jori, C. Abels, Photochem. Photobiol. Sci. 3 (2004) 907–917.
[22] P. Ran, W. Cao, H. Zheng, et al., Adv. Funct. Mater. 34 (2024) 2402731.
[23] F. Hu, G. Qi, et al., Angew. Chem. Int. Ed. 59 (2020) 9288–9292.
[24] G. Qi, F. Hu, et al., Angew. Chem. Int. Ed. 58 (2019) 16229–16235.
[25] W. Zhou, X. Da, Y. Jian, et al., Chem. Eur. J. 30 (2024) e202303766.
[26] Q. Cai, Y. Fei, H.W. An, et al., ACS Appl. Mater. Interfaces 10 (2018) 9197–9202.
[27] P.D. Ray, B.W. Huang, Y. Tsuji, Cell. Signal. 24 (2012) 981–990.
[28] D.B. Zorov, M. Juhaszova, S.J. Sollott, Physiol. Rev. 94 (2014) 909–950.
[29] F. Tian, Y. Jia, Y. Zhang, et al., Biosens. Bioelectron. 86 (2016) 68–74.
[30] H. Zhu, J. Fan, J. Wang, et al., J. Am. Chem. Soc. 136 (2014) 12820–12823.
[31] G. Cheng, J. Fan, W. Sun, et al., Chem. Commun. 50 (2014) 1018–1020.
[32] H. Guo, J.B. Callaway, J.P.Y. Ting, Nat. Med. 21 (2015) 677–687.
[33] G.J. Mao, Y.Y. Wang, W.P. Dong, et al., Spectrochim. Acta Part A 249 (2021) 119326.
[34] W. Gao, Y. Ma, Y. Liu, et al., Sens. Actuator. B: Chem. 327 (2021) 128884.
[35] M. Wu, W. Wu, Y. Duan, et al., Adv. Mater. 32 (2020) e2005222.
[36] L. Wang, J. Liu, M. Ren, W. Guo, Chin. Chem. Lett. 35 (2024) 108945.
[37] Z. Liu, K. Gao, B. Wang, et al., Sci. Rep. 6 (2016) 29065.
[38] X. Da, X. Liu, C. Li, et al., Chin. Chem. Lett. 34 (2023) 108317.
[39] Y. Xu, X. Da, L. Wang, et al., Chin. Chem. Lett. 36 (2025) 110168.
[40] Q. You, Medicinal Chemistry, 4th, Chemical Industry Press, Beijing, 2016.
[41] A. Hakonen, Anal. Chem. 81 (2009) 4555–4559.
[42] S. Goswami, S. Das, K. Aich, et al., Dalton Trans. 42 (2013) 15113–15119.
[43] A. Juris, V. Balzani, F. Barigelletti, et al., Coord. Chem. Rev. 84 (1988) 85–277.
[44] B.A. Lindig, M.A.J. Rodgers, A.P. Schaap, J. Am. Chem. Soc. 102 (1980) 5590–5593.
[45] C. Tanielian, C. Wolff, M. Esch, J. Phys. Chem. 100 (1996) 6555–6560.
[46] S.E. Gomez-Mejiba, Z. Zhai, M.S. Gimenez, et al., J. Biol. Chem. 285 (2010) 20062–20071.
[47] S. George, M.R. Hamblin, A. Kishen, Photochem. Photobiol. Sci. 8 (2009) 788–795.
[48] L. Ding, E.Y. Chi, K.S. Schanze, et al., Langmuir 26 (2010) 5544–5550.
[49] D. Yu, Y. Zha, Z. Zhong, et al., Sensors Actuators B: Chem. 339 (2021) 129878.